PAPER • **OPEN ACCESS**

In-situ monitoring for PBF-LB/M processes: Does multispectral optical tomography add value in recognizing process deviations?

To cite this article: Tina Becker *et al* 2023 *IOP Conf. Ser.: Mater. Sci. Eng.* **1296** 012008

IOP Conf. Series: Materials Science and Engineering 1296 (2023) 012008 doi:10.1088/1757-899X/1296/1/012008

In-situ monitoring for PBF-LB/M processes: Does multispectral optical tomography add value in recognizing process deviations?

Tina Becker[1], Philipp P Breese[1], Christian Metz[2] and Simon J Altenburg[1]

[1] Bundesanstalt für Materialforschung und -prüfung (BAM),
Unter den Eichen 87, 12205 Berlin, Germany
[2] ThetaScan GmbH, Thyssenstraße 183a, 46535 Dinslaken, Germany

tina.becker@bam.de

Abstract. Laser powder bed fusion of metallic components (PBF-LB/M) is gaining acceptance in industry. However, the high costs and lengthy qualification processes required for printed components create the need for more effective in-situ monitoring and testing methods. This article proposes multispectral Optical Tomography (OT) as a new approach for monitoring the PBF-LB/M process. Compared to other methods, OT is a low-cost process monitoring method that uses long-time exposure imaging to observe the build process. However, it lacks time resolution compared to expensive thermographic sensor systems. Monochromatic OT (1C-OT) is already commercially available and observes the building process layer-wise using a single wavelength window in the NIR range. Multispectral OT (nC-OT) utilizes a similar setup but can measure multiple wavelength ranges per location simultaneously. By comparing the classical 1C-OT and nC-OT approaches, this article examines the advantages of nC-OT (two channel OT and RGB-OT) in reducing the false positive rate for process deviations and approximating maximum temperatures for a better comparison between different build processes and materials. This could ultimately reduce costs and time for part qualification. The main goal of this contribution is to assess the advantages of nC-OT compared to 1C-OT for in-situ process monitoring of PBF-LB/M.

1. Introduction

The process of Laser Powder Bed Fusion of metallic components (PBF-LB/M) is an Additive Manufacturing (AM) technique, which utilizes a high-powered laser to melt metal powder across a powder bed. It enables the production of components with a high degree of design freedom directly from a CAD file. Despite its growing applications and usage of AM technology in industry, there is still a significant lack of understanding of the fundamental processes involved. Especially for applications in highly regulated industries, e.g., aerospace, cost and time extensive post-process non-destructive and destructive testing is needed to ensure component quality. Reliable monitoring systems could enhance the component reliability and save processing time and costs.

The substantial attention towards in-process monitoring for AM is shown in the high number of publications [1]. McCann et al. [2], AbouelNour and Gupta [3] and Grasso et al. [1] provide a good overview of the current state of research on the topic.

The occurring defects in the PBF-LB/M process can be divided into the categories: porosity, cracking, delamination, balling, geometric defects, surface defects, microstructural inhomogeneities and impurities [4]. Most of the defects are therefore caused by the extreme thermal gradients in the process. Due to this thermal character of the PBF-LB/M process, the thermal radiation emitted by the printed surface, mainly by the melt pool, is a good indicator for the process stability. It can be monitored by camera systems or photo diodes positioned outside the process chamber (off-axis) or integrated in the laser optical path (on-axis).

A promising on-axis monitoring approach to detect the surface temperature is the quotient pyrometry. Already in 2010 Pavlov et al. [5] could show that induced changes of the process parameters, e.g.

laser power and layer thickness, can be monitored reliably by a setup of two photo diodes equipped with different spectral filters in the scanning laser path. Very detailed shape and temperature information of the melt pool could be captured by Paul A. Hooper [6]. He presented an elaborated quotient pyrometric setup consisting of two on-axis positioned high speed cameras and equipped with spectral filters. The maximum occurring temperatures in the PBF-LB/M process could be shown to be significantly higher than the ambient boiling temperature of the used material titanium. Furumoto et al. [7] monitored a one-layer PBF-LB/M process by means of one high-speed camera equipped with a two-color radiometric thermal imaging system. They also could determine temperatures well above the ambient boiling temperature of the used powder material 18NI maraging steel.

On-axis quotient pyrometry delivers a good insight into the thermal PBF-LB/M process. However, expensive equipment and on-axis access to the PBF-LB/M machine is needed. In addition, a high amount of data of up to 40 Gbits/s [6] needs to be handled.

Optical Tomography (OT) is an off-axis thermographic approach using relatively simple equipment. Here, highly spatially resolved layer-images of the manufacturing process are taken by an off-axis positioned camera operating in the near infrared spectrum (NIR). This approach, described by Bamberg et al. [8], Zenzinger et al. [9] and Ladewig [10] enables a process monitoring with comparably low data volume. Compared to elaborated quotient pyrometry, information in the time domain is lacking. Guerra et al. could show that OT data can be used for detection of distortion of thin walls and lattice structures [11, 12]. Also lack-of-fusion defects could be correlated to OT data. [8] However, the information value of the greyscale images of the OT is limited since process inherent factors influence the measurement result as well as real process deviations [13, 14].

In this paper, the authors present a novel approach for process monitoring on basis of maximum temperature measurement: the multispectral Optical Tomography (nC-OT). The nC-OT is a method that combines the benefits of spatially resolved optical tomography with quotient pyrometry for surface temperature measurement in the PBF-LB/M process. Two different approaches were realized and tested on the in-house developed PBF-LB/M machine "SAMMIE": the two-channel optical tomography (2C-OT) and the RGB optical tomography (RGB-OT). This is the first time that an actual physical quantity, the maximum temperature, was deduced from data of a low-cost one camera OT system.

2. Approach

For each layer of the construction process (duration t_{layer}), one OT image is generated for each camera. To this end, the camera is in long exposure mode and several camera images of an exposure time $t_{exp} < t_{layer}$ are added together to form a single layer image, since t_{exp} is usually limited. Thus, the time history of the melting and cooling processes is lost, but the resulting amount of data is greatly reduced. Each resulting pixel value of a single layer image represents the sum of all emitted radiation at that surface point captured at the sensor area A of the camera at the viewing angle α.

The specific spectral radiance $M_\lambda(\lambda, T)$ of the melt pool can be calculated according to Planck's law as the product of the specific spectral radiance of an ideal black body M_λ^0 with the spectral angular emissivity $\varepsilon(\lambda, T)$ of the melt pool, see equation 1.

$$M_\lambda(\lambda, T) \cdot dA\, d\lambda = \varepsilon(\lambda, T) \cdot M_\lambda^0(\lambda, T) \cdot dA\, d\lambda \quad (1)$$

The signal intensity $I(T)$ of a monitoring camera can be calculated as a function of the temperature by integrating $M_\lambda(\lambda, T)$. Also, the spectral transmittance τ(λ) of the optical setup, e.g., lenses and filters, the spectral sensitivity S(λ) of the camera detector and a device specific correction factor c need to be considered. The real temperature curve of a surface point shows large temperature

gradients but can be assumed to be $T(t) = T_{max} \cdot \Delta t - t_{max}$in a first approximation. Equation 2 shows this correlation for one camera sensor.

$$I(T) = c \int \int \varepsilon(\lambda, T)\, M_\lambda^0(\lambda, T(t)) \cdot \tau(\lambda) \cdot S(\lambda) \cdot dt\, d\lambda \quad (2)$$

Thus, the temperature of the molten pool can theoretically be determined by using the numerical inversion of equation 2. However, since the course of time of the appearing temperatures and exact emissivity of the molten pool in the PBF-LB/M process is unknown and prone to unpredictable influences such as the oxidation-level of the surface and keyhole depression, this approach is unfeasible.

Here, as a first approximation, the monitored melt pool in the PBF-LB/M process is regarded as gray body. That means, the influence of the emissivity ε is not completely neglected but is considered as wavelength independent. Having simplified this, we decided to go for the quotient pyrometric approach, by using at least two different wavelength ranges for the process monitoring. Considering Stefan-Boltzmann's law, which states the dependence of the emitted radiant power on the temperature to the power of four, we can assume that the maximum occurring temperature T_{max} has by far the greatest influence on the recorded grey value. This is particularly true in the visible (VIS) and near infrared (NIR) spectral regions, used in the tested setups. Combining the quotient pyrometric approach with the gray body assumption and assuming the main influence by the maximum temperature T_{max} occurring, the ratio of two camera signal intensities can be calculated by equation 3.

$$I(T) = c\frac{\varepsilon(T_{max}) \cdot \int M_\lambda^0(\lambda, T_{max}) \cdot \tau_1(\lambda) \cdot S_1(\lambda)\, d\lambda}{\varepsilon(T_{max}) \cdot \int M_\lambda^0(\lambda, T_{max}) \cdot \tau_2(\lambda) \cdot S_2(\lambda)\, d\lambda} \quad (3)$$

This formula can be used to calculate the temperature of the melt pool using curve fitting via look-up-table, without knowledge of the emissivity. Having n different cameras/channels, $\binom{n}{2}$ intensity ratios can be determined in the same way for one surface point. By including several measurement values in the determination of the maximum temperature, measurement inaccuracies in individual channels can be better compensated. The reliability of the measurement can be improved.

3. Material and method

3.1. RGB Optical Tomography

The introduced RGB Optical Tomography (RGB-OT) setup is shown in figure 1a. A camera equipped with an RGGB Bayer filter, with a resolution of 24.4 megapixels and a pixel size on chip of 2.74 µm x 2.74 µm was used. Due to Planck's Law, a significantly higher proportion of spectral radiance can be expected at longer wavelengths. Therefore, the camera was equipped with a color balancing filter, reducing the intensity towards longer wavelengths. To further adjust the incident light, a neutral density filter was used. The setup was focused on the top-layer of the AM build process with a lens. To protect the sensor from the laser light (1070 nm), an additional low-pass filter with a cut-off wavelength of 750 nm was used.

The exposure time t_{exp} for the long-time exposure images was optimized and set to t_{exp} = 3 s to avoid saturation of pixels with unusually high dark current. The red, blue and one green channel of the camera were used for data analysis. The matching of the three datasets were achieved by simple superimposition. To reduce the optical distortion of the final dataset, a perspective transformation was performed.

3.2. Two channel Optical Tomography

For the two channel Optical Tomography (2C-OT) setup presented in this paper, two identical monochromatic CMOS cameras (C1 and C2 in figure 1c) with a resolution of 24.4 megapixels and a pixel size of 2.74 µm x 2.74 µm were used. These were each equipped with narrow band-pass filters in the NIR range (around 700 and 905 nm), and the fields of view were matched using a dichromatic long-pass beam splitter. To avoid ghost images induced by the beam splitter and to enable the option to insert and remove different optical filters without inducing focus shifts, an optical setup with parallel beam path was designed using a set of plano-convex lenses.

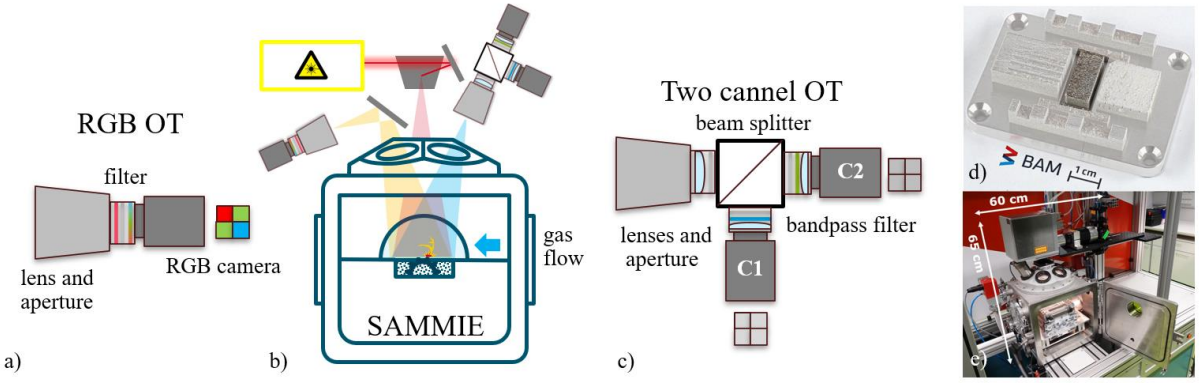

Figure 1. Setups used for the a) RGB-OT and c) 2C-OT presented, b) arrangement for the initial testing and e) image of the in-house developed PBF-LB/M machine "SAMMIE", d) monitored cuboid on the build plate

Similar to the RGB-OT setup, the exposure time t_{exp} for the long-time exposure images was optimized and set to t_{exp} = 3 s to avoid saturation of pixels with unusually high dark current. The two cameras were focused independently on the top-layer of the AM build process, accounting for the different optical focal lengths of the two different wavelength ranges. To further adjust the intensity of the incident light for both cameras, an aperture and several neutral density filters were used. The principle of the 2C-OT setup is illustrated in figure 1c. The generated datasets of both cameras were matched by affine perspective transformation.

The setup presented in this paper is a further development of a setup already described in [15] which has already been tested on a commercial PBF-LB/M system.

3.3. Calibration setup and calculation of the look-up table

Bias, dark, and flat frames corrections were performed for all images to minimize the influence of dark noise, readout noise and image errors such as vignetting [16]. The flat frames were created using an isotropic sphere (ED-ISS-100-MD, Gigahertz-Optik GmbH) and a calibrated halogen lamp (ISS-30-VA-V01, Gigahertz-Optik GmbH) with variable intensity setting, maintaining the colour temperature. The linearity of the used cameras was checked by means of the same setup.

The spectral transmittance τ(λ) of the used filters (bandpass, lowpass, temperature balancing filter, process windows) and lenses were measured by use of a spectrometer (OCEAN-FX-VIS-NIR-ES, Ocean Insight Inc.) in combination with the calibrated halogen lamp.

To correlate the measurement results of each setup to temperature values, the isotropic sphere with the calibrated halogen lamp was used as reference light source. The light source has a known spectral specific radiance $M_\lambda(\lambda)$ and a correlated color temperature T_{cal} = 3190 K in the visible range between 360 nm to 750 nm, when operated using the calibrated power settings. To have multiple supporting points, the light source was also operated with lower powers, resulting in lower color temperatures. By curve fitting of the spectral specific radiances $M_\lambda(\lambda)$, the corresponding color temperatures T_{color} were determined. These measurements provided the basis for the correction of the theoretically calculated correlations between measurement signals and temperature values.

3.4. Process setup

To test and compare both sensor setups at real process conditions, they were attached to the in-house developed sensor testing PBF-LB/M machine "SAMMIE", illustrated in figure 1b and shown in 1e. SAMMIE is equipped with an Ytterbium fiber laser with a wavelength λ_L of 1070 nm and maximum laser power P of 500 W, and has a build volume of 50 mm x 70 mm x 35 mm. The shielding gas flow direction of SAMMIE is marked with a blue arrow in figure 1b. Currently, four off-axis process windows and an on-axis access enable a simultaneous monitoring of the PBF-LB/M process with different optical sensor systems.

Both setups were connected to optical windows with a viewing angle of 22° to the build surface normal. The field of view of the RGB-OT was additionally guided by a silver mirror. For the 2C-OT, a sapphire process window was used, the RGB-OT was connected via a BK7 process window.

For the evaluation of the OT setups, the scanning process of a cuboid 30 mm x 8.5 mm x 25 mm sample, as shown in the middle of the build plate in figure 1d, was monitored. The component was built of 316L stainless steel and contains two sets of 12 cylindrical areas with diameters of d_{void} = 1.5 mm to 0.4 mm that were not illuminated to produce powder filled cavities as artificial defects. One set was built as a complete cylinder, on the other set the covering top was closed in a dome shape. The layer number 10 of the cuboid was scanned twice, to simulate double exposure scanning. Other components were printed in the same build job but are not focused on this paper.

A laser power P_L of 167 W, scanning speed v of 0.7 m/s, hatching distance l of 100 µm and layer thickness h of 40 µm were used as process parameters for the component. The laser spot diameter d_L was set to 80 µm. The monitored process was performed under argon atmosphere with a flow velocity of about v_{flow} = 3.5 m/s.

4. Results and Discussion

The generated look-up tables for the RGB-OT and 2C-OT are shown in figure 2a and 2b. Both figures show the correlation between measured surface temperature and detected intensity signal ratios. The continuous blue lines show the theoretically determined measured values. These were determined using Planck's law based on the measured transmission spectra of the optical elements and the sensitivity curves of the cameras.

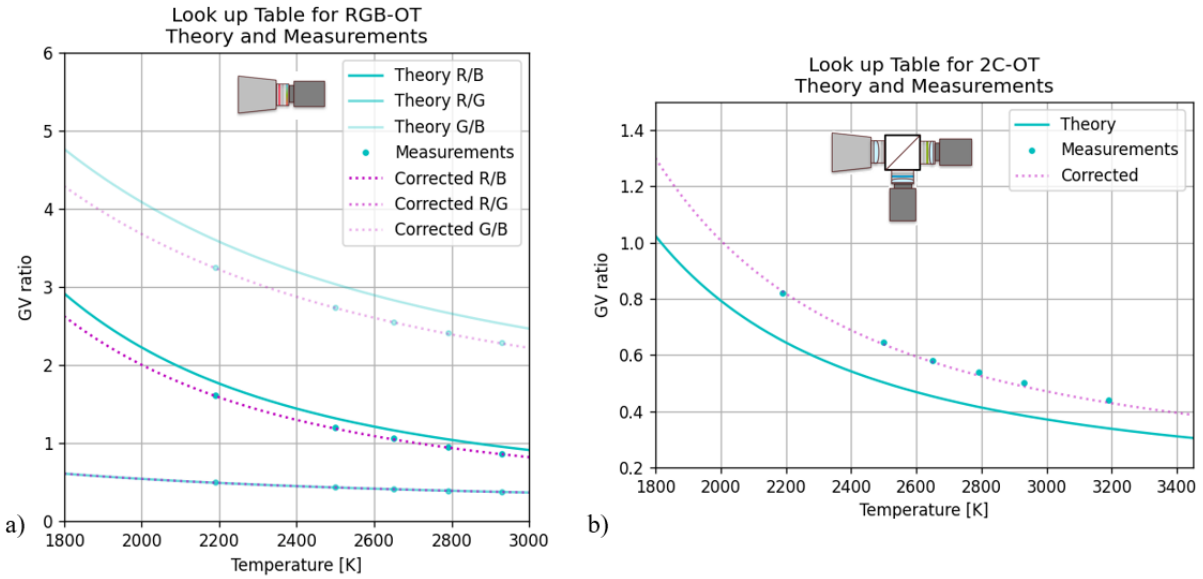

Figure 2. Look-up tables for the a) RGB-OT and the b) 2C-OT, both theoretical and corrected curves

The data points show the measured values obtained by means of the isotropic sphere with calibrated halogen lamp for different color temperatures. The purple dotted lines represent the final used

corrected curves of the look-up table after the determination of the specific correction factors. The corrected curve for the 2C-OT shows a good consistency with the measured values with maximum residuals e of $e_{2C} = \pm 0.013$. The RGB-OT corrected curves also show good agreement with residuals of $e_{R/B} = \pm 0.01$, $e_{R/G} = +0.003$ and $e_{G/B} = \pm 0.005$.

The deviation between the theoretical curve and the measured values of both RGB-OT and 2C-OT can be explained by the partly significant deviation D of the spectral composition of the radiation emitted by the calibrated lamp from the Planck spectrum, e.g. $D_{900nm} = 9$ % for the $T_{color} = 2290$ K. This deviation adds to the temperature measurement uncertainty and needs to be further investigated. However, due to the thermal calibration of the measuring systems, the measurement results can be considered correct.

A blackbody radiator as calibration source might give more reliable results. However, the emitted spectrum of many commercial blackbody radiators is only calibrated starting at about 800 nm and deviates significantly from the Planck spectrum in visible light range.

Figure 3 shows the measurement results of the two setups introduced in this paper and the underlying image data of the individual cameras/channels for an exemplary layer. The shown data was recorded during the production of the layer directly above the cylindrical cavities, i.e., the first completely exposed layer. The positions of the over-welds are marked on the sketch of the cuboid in figure 3c. The scanning lines of the laser are clearly visible in all images due to the high image resolution on the printing layer of 20 µm/pixel for the 2C-OT and 17 µm/pixel for the RGB-OT.

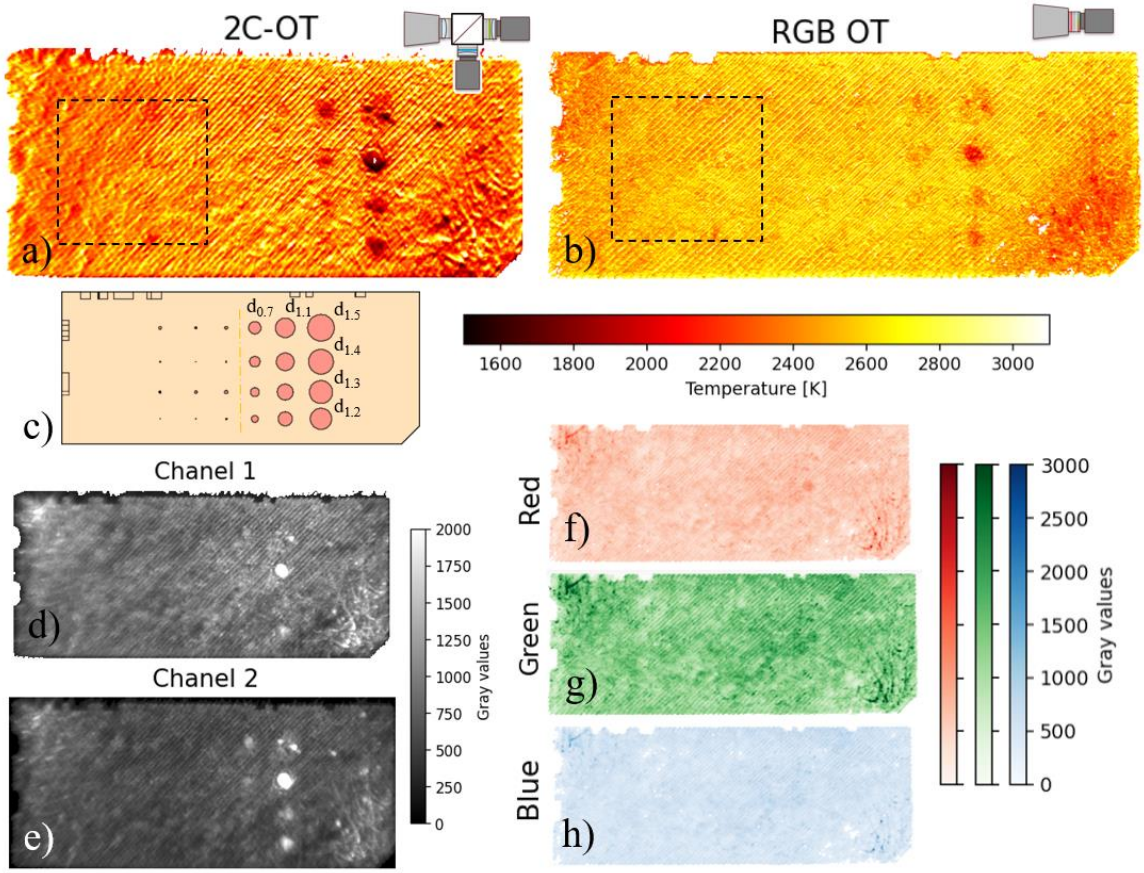

Figure 3. Measurement results of layer 71 directly above the embedded cylindric voids for the a) 2C-OT and the b) RGB-OT, corresponding images of d) channel 1 and e) channel 2 of the 2C-OT setup and the f) red, g) green and h) blue channel of the RGB-OT setup; c) sketch of the monitored cuboid

A comparison of the maximum temperature images of the two methods (figure 3a and 3b) shows a qualitatively good agreement. The averaged maximum temperature determined by the two methods are shown in table 1. The areas that were evaluated for this purpose are marked with a dotted contour in both images.

Table 1. Averaged maximum temperature determined by the RGB-OT and 2C-OT for the presented layer 91.

	Mean maximum temperature [K]	2σ [K]
RGB-OT	2550	370
2C-OT	2417	360

The maximum temperature measured for both systems is significantly above the melting temperature of the printed material 316L of about T_S= 1650 K but below the boiling temperature of about T_B = 2770 - 3086 K [17,18, 19]. The high values of the deviations of the measured maximum temperature of more than ± 370 K are expected due to the gaussian profile of the scanning laser, resulting in significantly higher energy input in the center of the scanned vector compared to the edges.

By use of a three-dimensional laser-keyhole welding model, Ki et al. [20] predict significantly higher maximum temperatures of 3600 - 4000 K, 500 - 900 K above the boiling temperature of the analyzed material iron in key-hole welding mode. Khairallah et al. [18] also suggest higher maximum temperatures of about 3000 K for a BPF-LB/M process of 316L using a fine-scale 3D simulation model. Ansari et al. [19] predicted temperatures of about 2800 K for a 316L PBF-LB/M process with similar process parameters using a Multiphysics simulation.

Using two-color pyrometric measurements, Pavlov el. Al. [5] determined surface temperatures in the range of 1173 – 2873 K for an PBF-LB/M IN625 process and Furumotoa et. Al. [7] reported surface temperatures between 1793 – 2083 K for an 18Ni stainless steel process. Pavlov et at. Used significant lower volumetric energy density of E_v = 44 J/mm³ compared to the E_v = 59 J/mm³ used in this paper. No detailed information is given for the process parameter experiment of Furumotoa et al.

To get an even deeper insight into the thermal history of the melt pool, more elaborate equipment, such as hyperspectral imaging, can be used. A detailed spatial temperature distribution and peak temperatures of over 2000 K for punctual laser welding of 316L stainless steel could be shown by Devesse et al. [21]. Similar temperature ranges could be shown for laser cladding of the same material by Lison et al. [22].

Thus, very different values for the maximum temperatures occurring in the PBF-LB/M process can be found in the literature. The authors of these papers agree that the maximum temperatures are highly dependent on the process parameters and the material used. The mean maximum temperature values determined with the setups presented here are very plausible and in the expected range. Still, further validation experiments are needed.

In figure 3a, the temperature image of the 2C-OT, most of the over-welded areas can be seen with the naked eye. In figure 3b, the temperature image of the RGB-OT, some of the over welds are visible as well. The over welds with diameters smaller than d = 0.9 mm, as well as the cavities with dome-shaped roofs cannot be distinguished. In the raw image data of the channel 2 (2C-OT), the image captured at the highest wavelength range, the over scanned areas are clearly visible down to a diameter of 0.9 mm. In all other raw images, just the defect with d = 1.4 mm diameter is clearly discernible. Consequently, for a monochromatic OT, the choice of the wavelength range in the upper NIR range is advantageous to observe these effects.

The mean temperature values of the two presented systems 2C-OT and RGB-OT over the height of the printed component are shown in figure 4b as well as the deviation between the two systems. The evaluated region of interest (ROI) on the part, a center positioned rectangle of 50 x 50 pixels is

marked in figure 4a. Correspondingly, the grey values of the underlying image data of the individual cameras/channels are shown in figure 4c and 4d. The temperatures detected by the RGB-OT are almost continuously higher than those of the 2C-OT. This small offset needs to be further investigated.

The fluctuations between the values of the different layers can probably be explained by the changing scanning angle with regard to the shielding gas flow. The grey values of the individual channels shown in Figure 4 have a variation of $2\sigma = \pm 38 - 48$ %. In contrast, the fluctuations of the presented nC-OT systems are only $2\sigma_{2C} = \pm 7.8$ % and $2\sigma_{2C} = \pm 7.2$ %. Thus, the influence of the shielding gas flow direction is greatly reduced using nC-OT. This phenomenon and the influence of the shielding gas flow on the PBF-LB/M process has already been described for the 1C-OT [23] but needs to be investigated further for all OT approaches. The origin of the variations is expected in the different absorption of thermal radiation by the welding plume, which depends on the relative orientation between plume direction (gas flow direction) and the scanning direction. Thus, a reduction of this effect is expected using ratio-based analysis, as done for the nC-OT

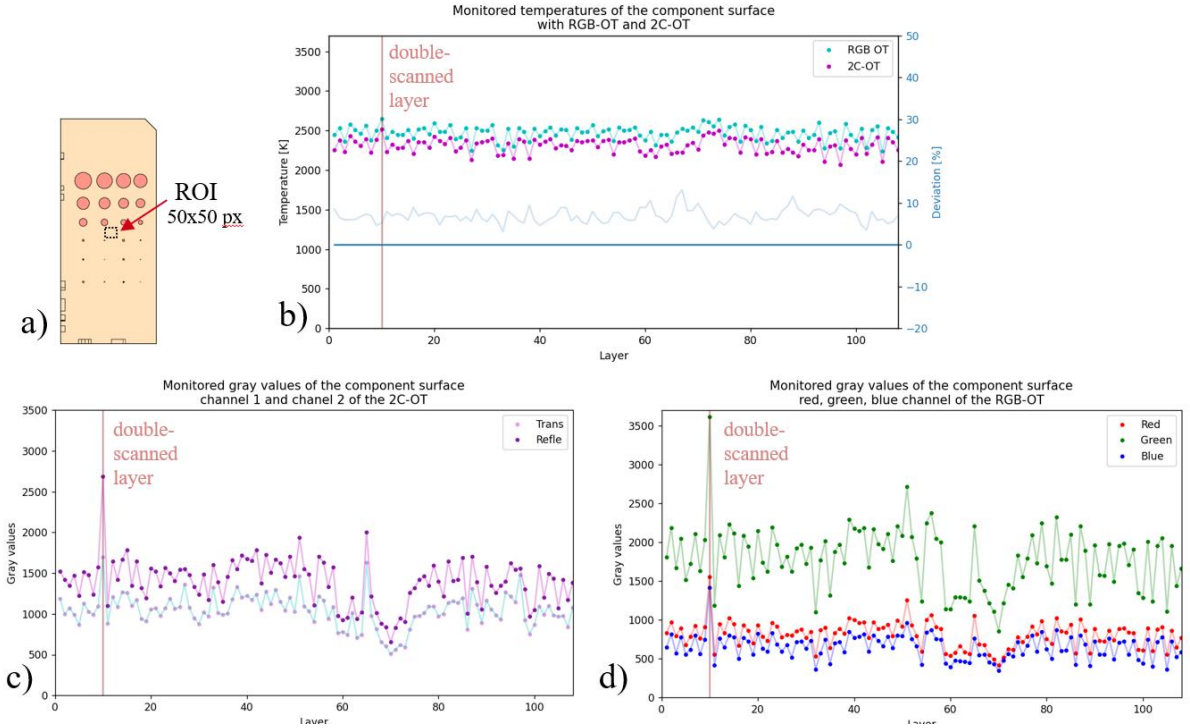

Figure 4. Mean temperature values of the a) centre region of the cuboid for the b) 2C-OT and RGB-OT with deviation information and corresponding mean grey values of the single channels of the c) 2C-OT and the d) RGB-OT

The red line indicates the layer with double exposure in figure 4b-d. The two presented systems did not record any excessive temperatures for the double-scanned layer ten. All single channels, on the other hand, show significantly higher values. This shows the ability of the two multispectral systems to distinguish between double-scanned areas and increased temperatures. This is especially advantageous, since local temperature deviations are expected to cause defects, while double exposures are frequently used, e.g., for contour scans, to improve the surface quality in standard PBF-LB/M processes.

The grey values of the individual channels also show deviating values in layers 60 to 70, the layers with the cavities, even though no changed scanning regime was applied at the ROI. In contrast, the temperature values of the two systems presented do not show any different behavior. It can be

assumed that the systems presented in this paper represent the actual temperature distributions better than single-channel systems.

5. Conclusion and Outlook

Two approaches for multispectral optical tomography - two-channel OT and RGB-OT - were introduced and first results of a feasibility study were presented. The spatially resolved temperature OT images obtained with the presented setups still need to be validated by comparative experiments, e.g., with thermocouples or other IR imaging methods. However, good agreement with literature values indicates that the results are very plausible.

By means of the two-channel OT, the two used narrow wavelength ranges can be optimally selected for the PBF-LB/M process. Since both camera sensors are used independently of each other, maximum spatial resolution can be achieved. However, the optical design is challenging and an image registration between the two channels has to be performed for data analysis. On the other hand, the RGB-OT setup is much simpler and more robust, off-the-shelf optics can be used and the results are still very promising.

It has also been shown that the two nC-OT systems are robust against apparent overheating in areas of double exposure, such as additional contour scans or as used for better attachment of components to the building platform. This is a common problem with 1C-OT systems. A higher robustness against false detections due to process radiation from other areas of the part was also demonstrated. Validation of these results, i.e., correlation with actual defects, is planned by means of reference CT measurements. The offset between theoretically determined curves and measurements that occurred during calibration, as well as the offsets between the two systems presented, will be investigated in more detail.

Further work will also investigate the influence of scan angle and shielding gas flow, by-products above the melt pool such as smoke and plasma plume, on the detected signal and component quality. With a better understanding and consideration of the occurring emissivity and the temporal shape of the temperature development during heating and cooling of the melt pool, we aim to improve the measurement results of our systems even more.

Since the PBF-LB/M process is already widely used in industry, economic efficiency and an easy implementation into existing industrial machines is very important. A reduction of the initial and operating costs, e.g., for the data storage, move even more into focus. Thus, the promising results of the presented systems show a great potential for future industrial applications.

Acknowledgment

Subsidized by the initiative QI-Digital.

Many thanks for the support in setting up our PBF-LB/M machine SAMMIE to Simon Oster, Jens Barow, Mathias Röllig, Jolanda Schumann and Tsuyoshi Shimada.

References

[1] Grasso M, Remani A, Dickins A, Colosimo B M and Leach R K 2021 *Meas. Sci. Technol.* **32** https://doi.org/10.1088/1361-6501/ac0b6b
[2] McCann R et al. 2021 *Additve Manufacturing* **45** doi.org/10.1016/j.addma.2021.102058
[3] AbouelNour Y and Gupta N 2022 *Materials & Design* **222** doi.org/10.1016/j.matdes.2022.111063
[4] Grasso M and Colosimo B M 2017 *Meas. Sci. Technol.* **18** doi.org/10.1088/1361-6501/aa5c4f
[5] Pavlov M, Doubenskaia M and Smurov I 2010 *Physics Procedia* **5** doi.org/10.1016/j.phpro.2010.08.080
[6] Hooper P A 2018 *Additive Manufacturing* **22** doi.org/10.1016/j.addma.2018.05.032
[7] Furumoto T, Oishi K, Abe S, Tsubouchi K, Yamaguchi M and Clare A T 2022 *Journal of Materials Processing Technology* **299** doi.org/10.1016/j.jmatprotec.2021.117384

[8] Bamberg J, Dusel K-H and Satzger W 2015 *AIP Conference Proceedings* **1650** doi.org/10.1063/1.4914605
[9] Zenzinger G, Bamberg J, Ladewig A, Hess T, Henkel B and Satzger W 2015 *AIP Conference Proceedings* **1650** doi.org/10.1063/1.4914606
[10] Ladewig A 2019 Optische Tomographie *PhD Thesis* Karlsruher Institut für Technologie
[11] Guerra M G, Lafirenza M, Errico V and Angelastro A 2023 *Optics & Laser Technology* **162** doi.org/10.1016/j.optlastec.2023.109252
[12] Guerra M G, Errico V, Fusco A, Lavecchia F, Campanelli S L and Galantucci L M 2022 *Additive Manufacturing* **55** doi.org/10.1016/j.addma.2022.102850
[13] Mohr G, Altenburg J S, Ulbricht A, Heinrich P, Baum D, Maierhofer C and Hilgenberg K 2020 *Metals* **10** doi.org/10.3390/met10010103
[14] Ulbricht A, Mohr G, Altenburg J S, Oster S, Maierhofer C and Bruno G 2021 *Metals* **11** doi.org/10.3390/met11071012
[15] Becker T, Altenburg S J, Scheuschner N, Breese P P, Metz C, Hilgenberg K and Maierhofer C 2022 *Procedia CIRP* **111** doi.org/10.1016/j.procir.2022.08.035
[16] Tomsik H Kalibrierung mittels Bias-, Dark- und Flatframe 2011 https://astrofotografie.fg-vds.de/grundsatzartikel.php
[17] Fischer U, Gomeringer R, Heinzler M, Kilgus R, Näher F, Oesterle S, Paetzold H, Stephan A 2011 Tabellenbuch Metall (Haan-Gruiten: Verlag Europa Lehrmittel)
[18] Khairallah S A, Anderson A T, Rubenchik A, King W E 2016 *Acta Materialia* **108** dx.doi.org/10.1016/j.actamat.2016.02.014
[19] Ansari P, Rehman A U, Pitir F, Veziroglu S, Mishra J K, Aktas O C, Salamci M U 2021 *Metals* **11** doi.org/10.3390/met11071076
[20] Ki H, Mazumder J, Mohanty P S 2002 *Metall. Mater. Trans. A* **33** doi.org/10.1007/s11661-002-0191-5.
[21] Devesse W, Baere D, Guillaume P 2017 *Sensors* **17** doi:10.3390/s17010091
[22] Lison M, Devesse W, Baere D, Hinderdael M, Guillaume P 2019 *Journal of Laser Applications* **31** doi: 10.2351/1.5096129
[23] Becker T 2020 Statistical analysis of optical monitoring data for layer wise defect detection in the LPBF process, *MSc Thesis* Technische Universität Berlin